Sensing Skin for Strain Monitoring Made of PC-CNT Conductive Polymer Nanocomposite Sprayed Layer by Layer

3 AUTHORS, INCLUDING:

Jean-Francois FELLER
Bretagne Loire University (UBL)
174 PUBLICATIONS **1,548** CITATIONS

SEE PROFILE

Mickael Castro
European University of Brittany
**95** PUBLICATIONS **762** CITATIONS

SEE PROFILE

Sensing Skin for Strain Monitoring Made of PC−CNT Conductive Polymer Nanocomposite Sprayed Layer by Layer

Colin Robert, Jean François Feller,* and Mickaël Castro

Smart Plastics Group, European University of Brittany (UEB), LIMAT[B]-UBS, Lorient, France

ABSTRACT: Sensing skins about 1.5 μm thick made of 40 nanolayers of conductive polymer nanocomposites (CPC) were sprayed layer by layer (sLbL) directly on a PET woven textile to demonstrate their versatility to monitor the deformation of a flexible, rigid and rough substrate such as a commercial boat sail. CPC sensing skins were developed by structuring a 3D carbon nanotubes network into three kinds of amorphous thermoplastic matrices (PMMA, aPS, PC). Adjustable parameters such as the thickness (number of sprayed layers) and the initial resistance of CPC transducers (CNT content relatively to percolation threshold) enabled to tailor both sensitivity and stability of the piezo-resistive responses, so that it was possible to monitor the strain evolution in the elastic domain and damage accumulation over this limit. Polymer matrices were selected after calculation of their χ Flory−Huggins parameters to evaluate their interactions with the PET substrate and solvent of dispersion, and after the comparison of their stress/strain characteristics, particularly their elastic limit. PC-1%CNT was found to be the best candidate satisfying both chemical and physical criteria. Finally, the exponential evolution of the piezo-resistive response of CPC sensing skins on a wide range of deformation (until breakage at ε = 27%), was well fitted with a model based on quantum tunnelling conduction inducing an exponential evolution of resistance with variations of CNT/CNT junction gap from 0.5 to 0.625 nm.

KEYWORDS: *strain sensing skin, piezo-resistive response, conductive polymer nanocomposite (CPC), carbon nanotubes (CNT), spray layer by layer (sLbL), Sail,*
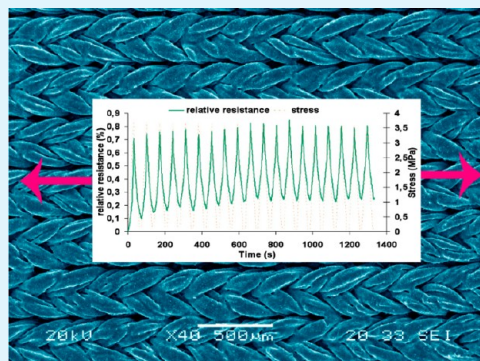
1. INTRODUCTION

After their first discovery in 1952 by Radushkevich et al.[1] and further popularization in 1991 by S. Iijima,[2] carbon nanotubes (CNT) have really created a breakthrough in nanotechnology. Actually, the exceptional intrinsic properties of CNT, such as electrical[3,4] and thermal conductivity[5] or mechanical properties,[6] has made them one of the most promising nanomaterials. On another hand, the progress in CNT mass production[7,8] nowadays allows for hopeful prospects in industrial fields such as transport, electronics, communication, and energy.[5,9] Although classical sensors were first made with semiconductors, solid electrolytes, insulators, metals, and catalytic materials, the adaptability and the development of conducting properties in polymer nanocomposites became prominent in the construction of sensor devices.[10] CNT Electrical properties combined to a high aspect ratio ($100 < L/D < 1000$) allowed the formation of a conductive network at very low concentration of filler compared to carbon nanoparticules for example.[11] Thus, because of their ability to form entanglements, CNT can be structured into light conducting networks when dispersed into a polymer matrix, leading to conductive polymer nanocomposites (CPC) sensors with accurate and reliable properties. Multifunctional smart applications of CNT based CPC were developed in numerous fields such as flow sensors[12] and volatile organic compounds (VOC) sensors for e-noses now used for anticipated cancer diagnosis[13,14] or toxic vapors
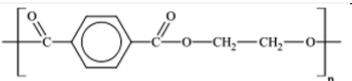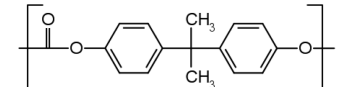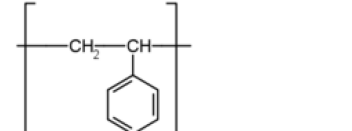
detection.[15,16] Strain sensors using carbon fibres were first investigated in the late 90s to monitor the strain and damage accumulation in thermoset[17,18] and thermoplastic[19,20] polymer composites. Since then, the incorporation of CNT in thermoplastic or thermoset resins revealed to be the main technique to monitor both deformation and health evolution of the structure. CPC are obtained by percolating conductive nanofillers[21−23] into an insulating polymer matrix. Additionally, from being highly sensitive to mechanical solicitations, they can also transduce environment variations like temperature[24,25] or VOC content in the atmosphere.[16,26] Their electrical responses were also found to depend on filler content and nature, matrix structure and properties, and making process. Different strategies can be used to develop CPC strain sensors with stable and reliable electrical responses, depending on the structure aimed: CPC cast film,[27,28] embedded CPC fibers,[29−31] CNT-coated polymer fibers,[32,33] in situ CVD growth on the structure,[34] and incorporation of CNT in the polymer matrix.[35−42] This strategy was widely reported[36,37] and modeled[38] by E. T. Thostenson et al. This bulk route has allowed researchers first to monitor the damage accumulation of the structure[39−41] and second to couple with the standard

Table 1. Melting Temperature T_m, Glass transition Temperature T_g, Density ρ, and Chemical Formula of Polymers

	T_m (°C)	T_g (°C)	ρ (g.cm⁻³)	Chemical formula
Poly(ethylene terephtahalate) PET [51]	250	82.5	1.34	
Poly(carbonate) PC [52]	amorphous	148	1.2	
Poly(methyl methacrylate) PMMA [16]	amorphous	109	1.2	
Atactic poly(styrene) aPS [43]	amorphous	100	1.05	

acoustic wave emission method.[42] However all these strategies make difficult to control the conducting network architecture of the strain sensing elements, as they depend on nanofillers dispersion and interconnection in the structure, which are difficult to control during the process. Recently, in 2005, we developed a versatile approach to assemble CPC sensors by spray layer by layer (sLbL).[43,44] Although it does not require any polyelectrolyte (and thus aqueous solution), the principle of this technique is similar to the electrostatic layer by layer (eLbL) popularized by J. Decher[45] in 1997. Since then, eLbL was adapted to nanocomposite-based on CNT[46,47] and montmorillonite[48,49] to build films from the assembly of nanolayers step by step. More recently N. Kotov et al. used these nanobricks to make sensing skins for spatial strain and impact damage identification[50−53] and T. Akter et al.[54] sprayed AgNW layers onto highly stretchable PDMS transparent films.

In this paper, we report the interest of using sLbL assembly to develop strain sensors under the form of thin films with large, stable and reliable electrical responses. This technique has many advantages among which: the possibility to disperse well CNT in many solvents and polymer matrices (not necessarily polyelectrolytes), the ability to make in situ sensing skins on almost all surfaces needing monitoring (with good adhesion), the step-by-step control of the formation of a hierarchically conducting architecture. The proof of concept has been done through the investigation of the strain sensing properties of CPC transducers sprayed onto woven sail specimen (a very irregular textile surface), in order to demonstrate their ability to be implemented into smart racing sailboats.

2. EXPERIMENTAL SECTION

2.1. Materials. Multiwall carbon nanotubes (NC-7000 MWNT) were kindly provided by Nanocyl (Belgium). This grade corresponds to MWNT with an average diameter of 10 nm and a mean length between 100 and 1000 nm. LEXAN 141R poly(carbonate) PC was purchased from GE Plastics (France). Poly(methyl methacrylate) PMMA VQ 101S was purchased from Rohm (Germany). Flakes of atactic poly(styrene) aPS were purchased from Polyscience (France) with an average molar mass of $\bar{M}_M$ = 50 000 g mol⁻¹. The thermal characteristics and chemical formula of polymers are given in Table 1, whereas some of their mechanical properties are summarized in Table 2. Chloroform was provided by Aldrich (France), stabilized with

Table 2. Mechanical Properties of Polymers in the Elastic Domain (from Figure 3)

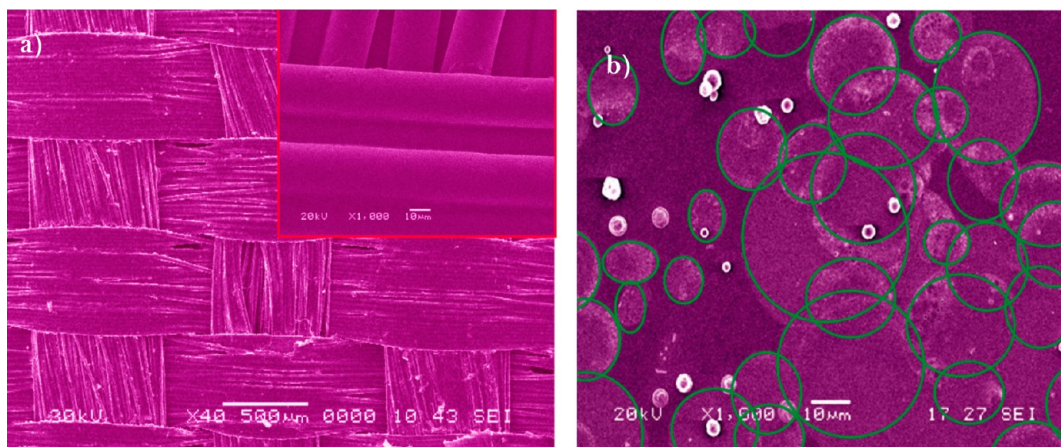|	E (GPa)	σ_e (MPa) limit of elasticity	ε_e (%) limit of elasticity	ε_e (%) at break
PET Mylar sail	3.852	40.4	1.05	26
aPS	3.22	13.8	0.43	0.66
PC	2.31	14.8	0.64	2.1
PMMA	2.88	14.7	0.51	0.95

amylenes with a purity superior to 99%. The sail Soft Norlam samples were kindly provided by NorthSails (France). This sail is composed of a Mylar sheet in sandwich between two layers of woven poly(ester) textile. The Mylar sheet is a biaxially orientated poly(ethylene terephtalate) (bo-PET). This core layer is a key component of laminates because it combines low stretch and lightweight at a reasonable cost. The Soft Norlam sail looks like a woven textile sail because the Mylar film is hidden between two light, tough layers of woven polyester fabrics (see Figure 1a). The Mylar's low stretch bolsters the fabric omnidirectionally, allowing the woven yarns to carry load in the primary strain directions (which the designed panel layout carefully matches), while limiting distortion in off-thread line.

2.2. Dispersion of CNT in Solution. The polymer was first dissolved in chloroform, and then CNT were added (all percentages in the following are in weight if not specified). The concentration of polymer-CNT CPC was 10 g dm⁻³ of solvent. CPC solutions were homogenized by sonication with a Branson 3510 sonicator for 90 min at 25 °C, and further degassed for 5 min. Chloroform was chosen mainly because, according Hansen's parameters, it will dissolve the different thermoplastic polymers used and well disperse CNT.[55] The van Krevelen[56] method was used to calculate Hansen solubility parameters.[57] The solubility parameter δ_t (eq 1) is calculated from the dispersive forces δ_d (eq 2), the polar δ_p (eq 3) and the hydrogen δ_h (eq 4) components.

$$\delta_f^2 = \delta_d^2 + \delta_p^2 + \delta_b^2 \tag{1}$$
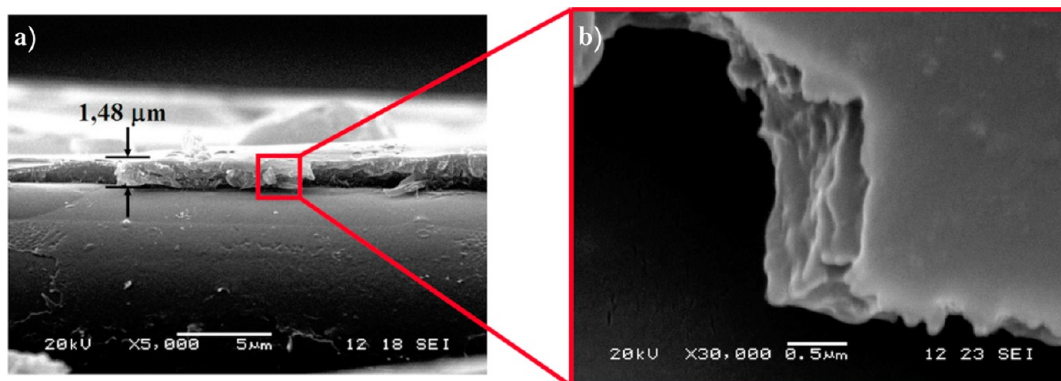
$$\delta_d = \frac{\sum F_{dG}}{V} \tag{2}$$

$$\delta_F = \frac{\sqrt{\sum F_{pi}^2}}{V} \tag{3}$$

Figure 1. (a) Texture of Soft Norlam sail coated with 40 layers of PC-1%CNT (inset shows a magnification of CPC coating on the sail fibers), (b) morphology of PC-1%CNT μdroplets welded by evaporation after spraying 1 layer.[16].

Table 3. Hansen Solubility δ (eq 1) and Flory−Huggins χ (eq 6) Parameters for Polymers and Chloroform

	δ_t (J cm^{-3})$^{1/2}$	δ_d (J cm^{-3})$^{1/2}$	δ_p (J cm^{-3})$^{1/2}$	δ_h (J cm^{-3})$^{1/2}$	mol vol (cm^3 mol^{-1})	χ/CHCl$_3$	χ/PET
CHCl$_3$	**19.0**	17.8	3.1	5.7	80	0	
aPS	**18.0**	18.0	1.1	0.0	98	0.0268	1.1325
PC	**20.1**	18.7	2.9	7.0	203	0.0487	0.3258
PMMA	**20.2**	17.0	5.8	9.2	84	0.054	0.3202
PET	**22.7**	19.7	4.3	10.3	131.4	0.44	0

Figure 2. Cross-section view of Soft Norlam sail coated with PC-1%CNT 40 layers: (a) investigation of the thickness of CPC, (b) sLbL structure on Soft Norlam polyester fiber.

$$\delta_{\dot{d}} = \frac{\sum F_{ki}}{V} \tag{4}$$

Where V is the molar volume of the polymer, and F_{di}, F_{pi}^2, and E_{hi} are intrinsic properties related to their structural groups.

Then Flory−Huggins interaction parameters χ calculated from eq 5 were investigated to show the solubility of the studied polymers in chloroform.

$$\chi = \chi_H + \chi_S \tag{5}$$

In polar systems, the value of $\chi_S = 0.34$ is generally used for the entropic contribution.[55] The enthalpic contribution (χ_H) is related to the molar volume V (dm^3 mol^{-1}), the temperature used (K), the gas constant R (J K^{-1} mol^{-1}), and the Hansen parameters of the polymer (δ_1) and of the solvent (δ_2), summarized in Table 3, according to eq 6.

$$\chi_H = \frac{Vs}{RT}(\delta_1 - \delta_2)^2 \tag{6}$$

The state of dispersion is also related to the degree of polymerization of macromolecules that will condition their mobility. To allow an effective dispersion, the χ parameter must be under 0.5 for a polymer with an infinite degree of polymerization. According to Flory−Huggins theory, all systems will easily be soluble thanks to their low enthalpic parameter.

2.3. Spray Layer by Layer (sLbL) Process. Sensing skins were processed by spray layer-by-layer (LbL) deposition technique from CPC solutions previously fabricated as described in previous works.[58−62] CPC solutions were sprayed directly onto sails layer-by-layer with a homemade device allowing a precise control of nozzle scanning speed (V_s = 10 cm s^{-1}), solution flow rate, stream pressure (p_s = 0.20 MPa), and target to nozzle distance (d_{tn} = 8 cm). During solvent evaporation, CPC μdroplets of 15−60 μm (Figure 1b) can weld to form a hierarchical 3D percolated network.[16] Between 10 and 40 layers (of 35 to 40 nm thick) were deposited on samples surface to make a skin of up to 1.5 μm thick (see Figure 2).

2.4. Tension Tests and Electrical Measurements. For the determination of basic mechanical properties of potential polymer matrices for CPC skins, samples were cut out hot pressed films, to obtain a standardized dog bone shape of 400 μm thick, 4 mm wide and 30 mm long (effective zone). An Instron 5566A was used at a speed of 1 mm.min^{-1}. Tests were repeated on 6 samples for each polymer type. For the determination of piezo-resistive properties of CPC skins, tests

3510

dx.doi.org/10.1021/am300594t | ACS Appl. Mater. Interfaces 2012, 4, 3508−3516

were done on a MTS Synergy RT/1000 tensile machine. Cyclic solicitations were performed on sail samples at a speed of 0.2 mm min^{-1} up to 0.6% deformation and 20 cycles have been done at 0.2 mm min^{-1} loading/unloading speed. A pretension of 20 N was applied. Electrical measurements were performed with a Hioki 3522−50 LCR device in direct current (DC) at a monitoring voltage of 1 V.

3. RESULTS AND DISCUSSION

3.1. Design of Transducers. The design of sensors has been optimized by changing the polymer matrix nature and further on transducers' thickness by adjusting the number or sprayed layers and the CNT content in the selected matrix. All polymer matrices chosen for the CPC transducer's were amorphous to facilitate the interpretation of behaviors and get rid of any undesirable effects coming from crystallinity changes on sensing behavior.

The choice of the polymer matrix has an undeniable influence on transducers properties although it must be a compromise between sensitivity to strain, linearity in the considered range of deformation, adhesion with PET substrate and solubility in chloroform to ensure a good ability to spray. Figure 3 shows the classical stress/strain curves of the three
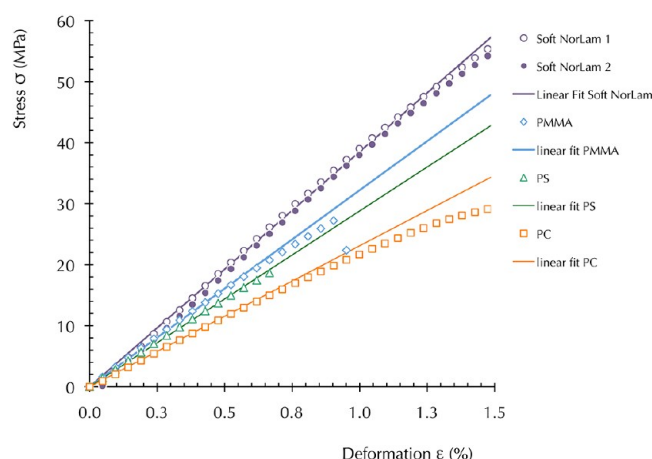

Figure 3. Stress/strain characteristics of films (150 μm thick) of possible transducers' matrices, PMMA, aPS & PC compared to that of Soft Norlam sail.

polymer matrices, PMMA, aPS & PC compared to that of Soft NorLam sail made of Mylar PET. The most relevant parameters for this study are the stress and strain at the limit of elasticity (determined when the slope used to calculate the Young's modulus drops) and strain at break, they are collected in Table 2. All polymers envisaged for the transducer's matrix have almost the same stress at the limit of elasticity but PC despite a slightly lower modulus, has the largest limit of elasticity (0.64%) and strain at break (2.1%). These mechanical characteristics are reasonable considering the working range of deformation of the PET sail provided by the manufacturer (0.6%). The fact that all mechanical characteristics of polymer films are lower than what can be expected from the literature (although experiments were repeated with 6 samples of each grade and found reproducible) must come from the small dimensions of samples (particularly their thickness). However, once formulated with CNT and sprayed, PC matrix allows to follow deformations up to 25% although plastically deformed (see Figure 9). Moreover, this suggests that the limit of sensing with thermoplastic polymer matrices does not come from

quantum tunnelling but from its plasticity or fracture. Additionally, measuring the deformation of a woven textile requires special clamps and a preload of 50 N, thus it is complicated to give a value of minimum measurable strain with our sensors. However Figure 6 suggests that this limit is close to 0.03% deformation. Finally these characteristics were found suitable to monitor the deformation of a PET sail, which has a higher modulus, elastic limit and strain at break, but a practical range of strain in use that must be kept under 0.6%. Moreover, the values of the interaction parameters between polymer matrices and their substrate calculated from eq 6 and collected in (Table 3) are all frankly under 0.5 suggesting a good adhesion with PET, in particular for PC χ = 0.0487. The amplitude of responses Ar (defined in eq 7) of the three different CPC sensors, obtained by spraying 20 layers of aPS, PMMA & PC filled with 1%CNT onto sail's samples are compared in Figure 4a. The increase in both initial resistance R_0 and relative resistance amplitude Ar from PC, PMMA to aPS can be explained by their different levels of dispersion of CNT, resulting from their different mutual affinities. However, although aPS matrix seems to lead to the most sensitive CPC skin, in practice PC leads to the best compromise between sensitivity and stability of signals. Additionally the preferred R_0 is generally targeted between kΩ and MΩ, making PC a good candidate. Furthermore, panels b and c in Figure 4 show that the sensitivity of PC−CNT transducers can be post-tuned by adjusting CNT content (acting on percolation) and the number of sprayed layers (acting on thickness) respectively, which finally can partly compensate the lower initial sensitivity of PC compared to other matrices. But it must also be noted that when films become too thick (by increasing to much the number of sprayed layers) or contain to much CNT, this results in a larger amount of conducting pathways, which increase the CPC sensor's conductivity and stability but also decreases its sensitivity. This preliminary study has demonstrated the great versatility of CPC films assembled by sLbL due to the many adjustable parameters that allow to tailor their piezo-resistive properties. However, PC-1%CNT (20 layers) is certainly the CPC leading to the best compromise between all chemical and physical requirements previously mentioned. Let us have a look to the morphology of the multilayer films constituting the transducers and the way they are assembled to the substrate (sail).

3.2. Morphologies' Observation by Scanning Electron Microscopy (SEM). Figures 1 and 2 show the microstructure of CPC sprayed sail fabrics observed by SEM. At low magnification one can clearly see the rough weft of the textile, but constituted of well-woven polyester μfibres. However, at larger magnification (Figure 1a inset) the fibres surface appears smoother, which confirms the homogeneity of the sprayed LbL coating, and it is also possible to determine that their diameter is about 30 μm. Moreover, the cross-section of a coated fiber after breakage (Figure 2a) shows that the thickness of 40 layers of PC-1%CNT is about 1.5 μm. Additionally, zooming on the coating profile (Figure 2b) reveals the sLbL structure of the sensing skin, each layer has thus an average thickness of 40 nm, which confirms previous measurements.

3.3. Nonreversible Piezo-Resistive Response. The piezo-resistive effect of the sensing skin results from the promotion of quantum tunnelling conduction in the CPC transducer to the detriment of classical ohmic conduction.[63−69] Therefore, when the sensors are strained at the macroscale, the average interparticles distance (gap) in the percolated network
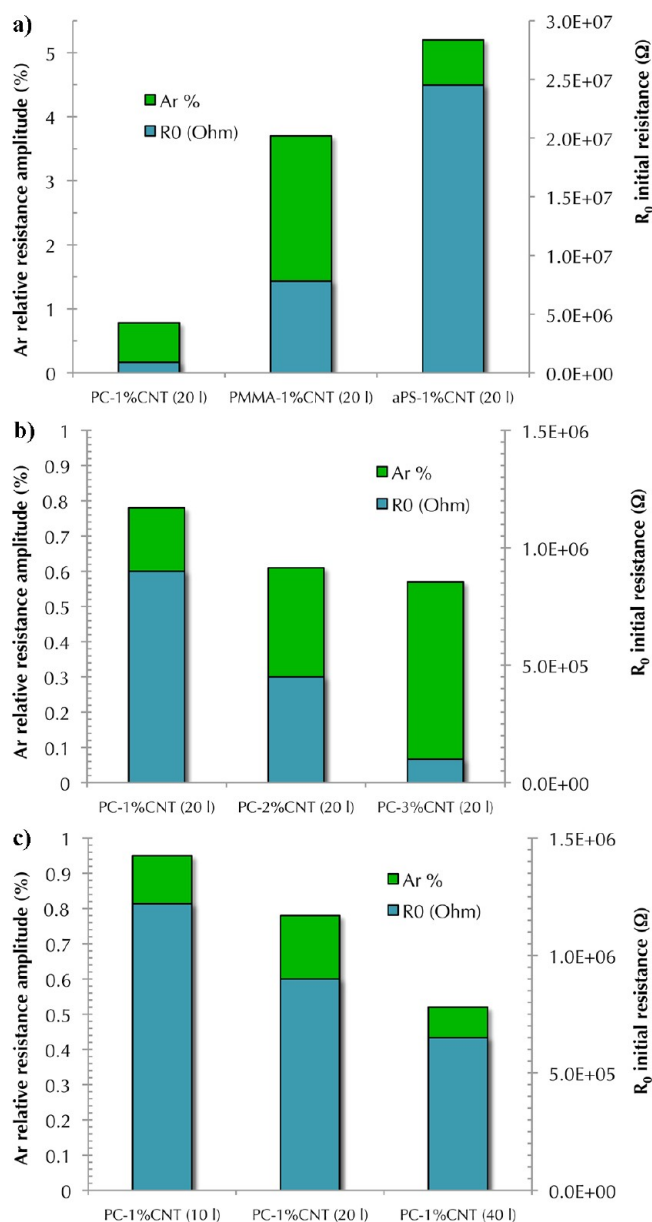
Figure 4. Influence of transducers' polymer matrix nature on their a) A_r (response amplitude, see eq 7) and R_0 (initial resistance) for 20 sprayed layers and PC, PMMA & aPS filled with 1%CNT, b) Influence of CNT content on A_r and R_0 for PC matrix and 20 sprayed layers. (c) Influence of transducers thickness on A_r and R_0 for PC-1%CNT.

relaxations and slipping with increasing deformation amplitude from a cycle to another. This is well evidenced in Figure 5a where the breaks in curves of A_r suggest that each new cycle is keeping the memory of the deformation of the previous one.

$$A_r = \frac{\Delta R}{R_0} \tag{7}$$

where R_0 is the initial resistance without load
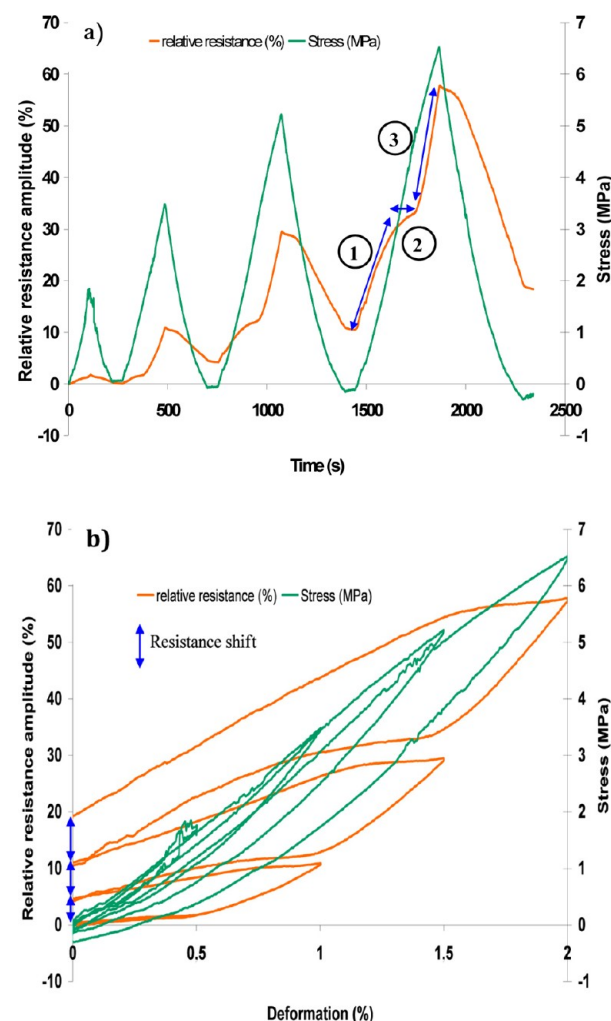
Figure 5. PC-1%CNT (40 layers) submitted to strain sweep from 0 to 2% by increments of 0.5%. (a) Evolution of stress and relative resistance A_r with time, (b) evolution of A_r and stress with deformation and initial resistance R_0 shift.

increases accordingly at the nanoscale. The interesting peculiarity of electrons' hopping conduction is its exponential dependency with the average gap between CNT that is providing the CPC material with high sensitivity toward mechanical solicitations. Thus, only several tenths of nanometres of displacement of nanofillers at junctions will induce a global resistance increase, proportional to the total number of disconnected conductive pathways. In the elastic domain of the sensor's matrix, the piezo-resistive signal is reproducible upon loading/unloading cycling unless the polymer of the substrate (here PET fibres from the sail) is reaching its plastic domain. In this case, a nonreversible phenomenon will take place due to creep and the transducer's response A_r (A_r is also called relative resistance amplitude and defined by eq 7) will present discontinuities resulting from the accumulation of chains

Thostenson et al.[40] have also reported a similar behavior in glass fiber/epoxy−CNT composites. In both cases, the woven structure (glass or polyester fibres) is mainly supporting the load. The unidirectional tensile effort is thus inducing micro displacements of fibres perpendicularly to the mechanical solicitation. Nevertheless, in their case the transducer is the CNT network in the core of the epoxy resin whereas in ours the sensing skin is on the surface of a sail composed of a film in sandwich between two fabrics. Therefore the mechanisms observed must be rather different although concerning damage of fibres and matrices. However, in all cases a nonreversible behavior is observed, which is evidenced in our case by the nonrecovery of initial resistance value during unloading,

3512

dx.doi.org/10.1021/am300594t | ACS Appl. Mater. Interfaces 2012, 4, 3508−3516

suggesting the persistence of a residual strain clearly observed in panels a and b in Figure 5. Thus, following A_r baseline's drift along cycles in panels a and b in Figure 5 is a good way to quantify the damage accumulation as a function of strain amplitude increase. However, this phenomenon is very limited in the first cycle, as for only 0.5% of strain, almost no drift in A_r baseline is observed in Figure 5b; this suggests that both polymers of sensor and sail are still in their elastic domain of deformation. A finer analysis of curves reveals a three steps process in the damage. During the initial stage, it seems that only undamaged areas are responding, whereas over the strain value of the previous cycle, new damages occur until the unloading and until the final breakage of the sail sample. To prevent such nonreversible behaviors to take place and to ensure an optimal reproducibility of sensor's responses during cycling, we kept the range of deformation under the limit of elasticity of all polymers, i.e., 0.6%, as recommended by the sail's manufacturer.

3.4. Reversible Piezo-Resistive Responses. To verify the reversibility of sensor's response in tensile mode, we submitted samples to linear increase/decrease of strain in the elastic range, and checked the synchronism of piezo-resistive and stress responses. Figure 6a illustrates the piezo-resistive behaviors of PC-1%CNT transducers, assembled to sail samples, in the elastic domain of deformation. After few solicitations, the baseline is quickly stabilizing. The deformation of textiles being complex, the fibres' alignment in the main axis, sliding effects and stresses from fibres perpendicular to the direction of solicitation are assumed to be responsible for the residual deformation of the sail's samples during the first cycles. Figure 6b, provides another angle of analysis, as the piezo-resistive response is expressed directly versus deformation. It is now very
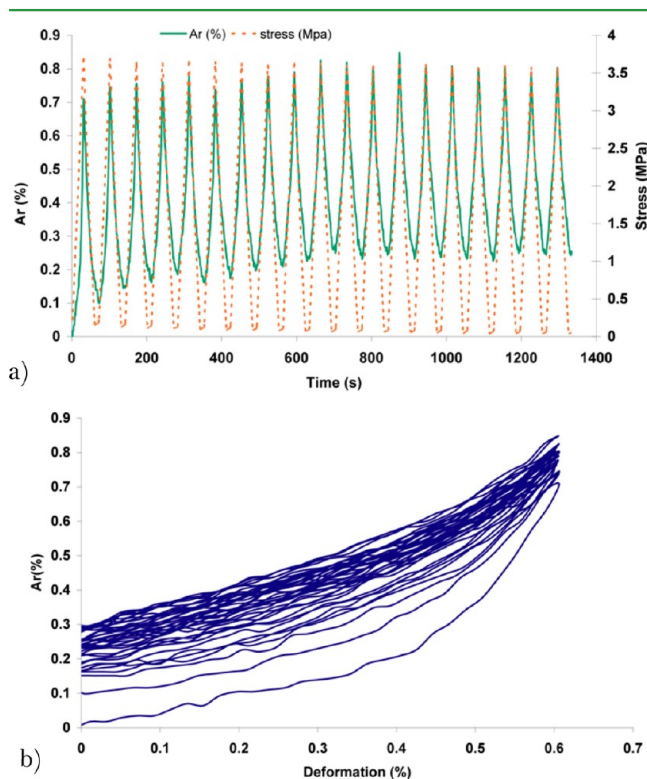
Figure 6. Piezo-resistive behavior of PC-1%CNT (40 layers): (a) synchronism of A_r with stress versus time; (b) drift of A_r/stress curves along cycling.

clear that signals loose their linearity when the limit of the elastic domain is reached, i.e., close to 0.65% of deformation. The weak hysteresis of loading/unloading loops is also a good illustration of the reversibility and reproducibility of sensors' responses with time. However on longer periods of solicitation, more than 400 cycles (23 h), the evolution of the response amplitude Ar shows an initial decrease of 0.15% during the first 3 h followed by a stable plateau lasting until the end of the test (20 h). Moreover, taking the first linear part of the curves to calculate the gage factor (GF) with eq 8 give a value of GF # 0.7, which is 3 times less than standard metallic gages. However, the same evaluation in the second part of the curve between 0.45 and 0.6 leads to GF = 2.5 thus demonstrating the interest of CPC skin gages. Furthermore, in the plastic domain illustrated by Figure 9, GF as high as 100 can be reached.

$$GF = \frac{\frac{\Delta R}{R}}{\Delta \varepsilon} \tag{8}$$

The versatility of sprayed CPC skins is furthermore demonstrated through their application on other kind of textiles of different structure and nature, such as cotton in Figure 7 or Lycra (PU) in Figure 8. Although the responses obtained with cotton substrate are typical those of Lycra substrate are anomalous (double peak out of phase) but conform to what was found by some other authors with Spandex (another PU), i.e., R. Zhang et al.[32] This peculiar behavior is still not completely elucidated but may certainly come from the important deformation of 35% used and from the complex solicitations resulting from such deformation of the textile.

3.5. Origin of Piezo-Resistive Response of CPC Strain Sensors. Provided that the amount of CNT in the polymer matrix is properly chosen just over the percolation threshold, the dominant factor responsible for the resistance variation will be quantum-tunnelling current. The interest of promoting such mode of conduction is that the resistance of the CNT percolated network becomes proportional to the average gap (s) at CNT/CNT junctions. Thus any macro-deformation of the sensors will result in exponential variations of resistance with tiny gap variations of some fractions of nanometres. Several authors have modeled the piezo-resistive behavior of CNT network during strain sensing depending on key parameters affecting signals such as: CNT content,[63−68] CNT arrangement,[66,67] polymer matrix nature,[65,68] and damage accumulation.[69] In these models, the total electrical resistance of CPC is assumed to be function of both conductive filler and polymer matrix resistances. Because the resistance of fillers is very small beyond that of the polymer matrix, the resistance across particles is neglected. Moreover, quantum tunnelling current is expected to affect only places where inter CNT gap is smaller than the cut off distance.[63] To achieve the comprehension of the tunnelling effect, Zhang et al. modeled the statistical percolation transition of randomly dispersed conductor particles in an insulating matrix.[70] Teteris et al. showed the reliability of that model on both carbon nanoparticules[71,72] and CNT.[73] According to this model, the total resistance in a nanocomposite is expressed by eq 9

$$R = \left(\frac{L}{N}\right)\left(\frac{8\pi hs}{3a^2 \gamma e^2}\right)e^{(\gamma S)} \tag{9}$$

Where L is the number of particles forming a single conductive path, N the number of conducting paths, h the Plank's constant,
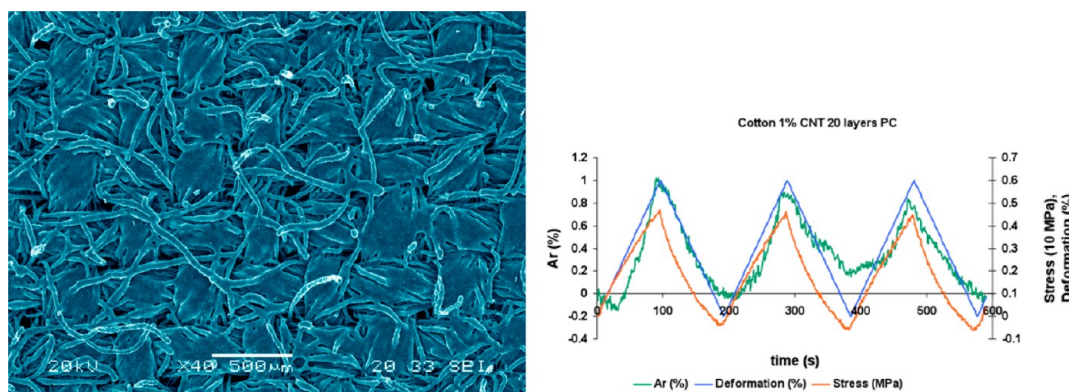
Figure 7. (Left) SEM of PC-1CNT (20 layers) skins sprayed onto cotton, (right) piezo-resistive response of the same sensor.
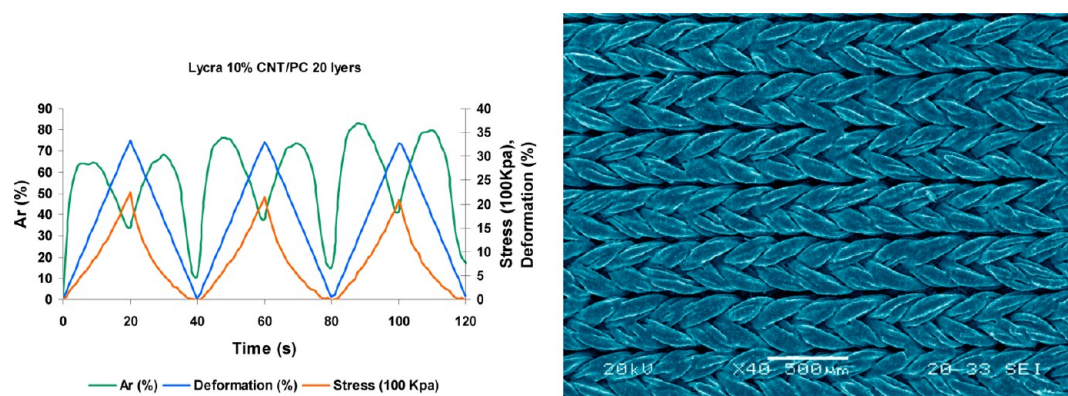

Figure 8. (Right) SEM of PC-1CNT (20 layers) skins sprayed onto cotton, (left) piezo-resistive response of the same sensor.

s the least distance between conductive particles, a^2 the effective cross-section, where tunnelling occurs, e the electron charge, and γ is calculated with eq 10

$$\gamma = \frac{4\pi(2m\phi)^{0.5}}{h}$$

(10)

Where m is the electron mass and ϕ the height of potential barrier between adjacent particles.

The composite strain increases the resistance thanks to the modulation of inter particle length. The particle separation changes from s_0 to s, and shows a relative resistance (R/R_0) given by eq 11:

$$\frac{R}{R} = \left(\frac{S}{S_0}\right)e^{r(s-s_0)}$$

(11)

Where R_0 is the initial resistance, and s_0 the initial inter particles length.

Assuming that the deformation is uniform between CNT and polymer matrix, the inter particle distance s under tensile strain is given by eq 12

$$S = S_0(1 + \varepsilon) = \left[1 + \left(\frac{\Delta l}{l_0}\right)\right]$$

(12)

Where ε is the tensile strain of the polymer matrix, Δl the deformation of composite sample, and l_0 the initial length of the sample.

Substitution of eq 12 into eq 11 yields eq 13:

$$\ln R = \ln R_0 + \ln\left[1 + \left(\frac{\Delta l}{l_0}\right)\right] + \gamma S_0\left(\frac{\Delta l}{l_0}\right)$$

(13)

Figure 9 is very clearly evidencing that PC-1%CNT (40 layers) piezo-resistive behavior is following an exponential law from 0.6
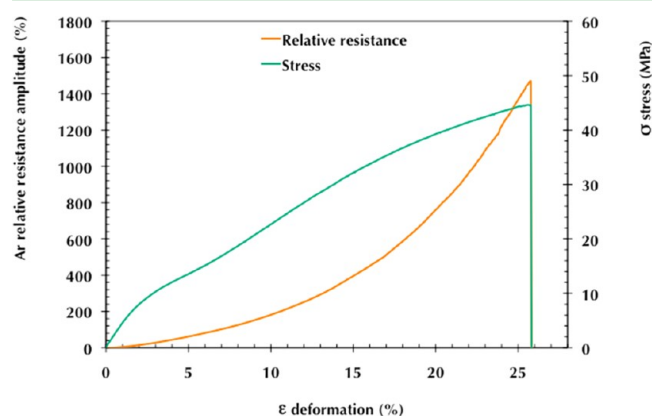

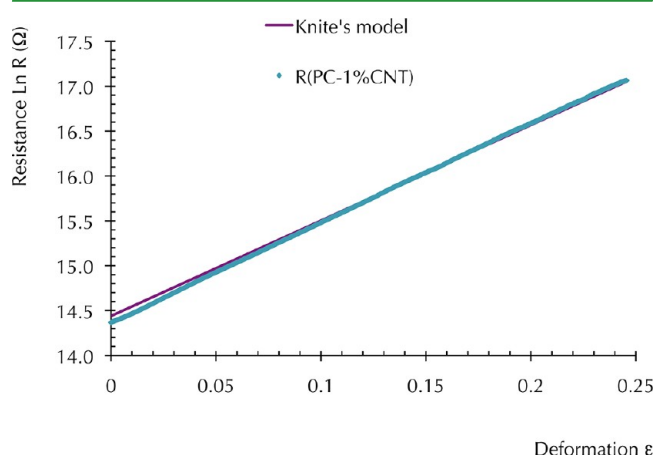**Figure 9.** PC-1%CNT (40 layers) sample until breakage.

to 27% of deformation, which corresponds to the breakage of the sensing skin. This phenomenon is clearly evidenced by SEM in Figure 10, which allows to compare the morphology of the sensing skin before and after its fracture. The damage appears to be located at the crossing of two strands, where stresses must be concentrated. The peculiar texture of the surface showing craters remaining from solvent evaporation is also visible. Moreover, Knite's model was successfully used to

3514

dx.doi.org/10.1021/am300594t | ACS Appl. Mater. Interfaces 2012, 4, 3508−3516
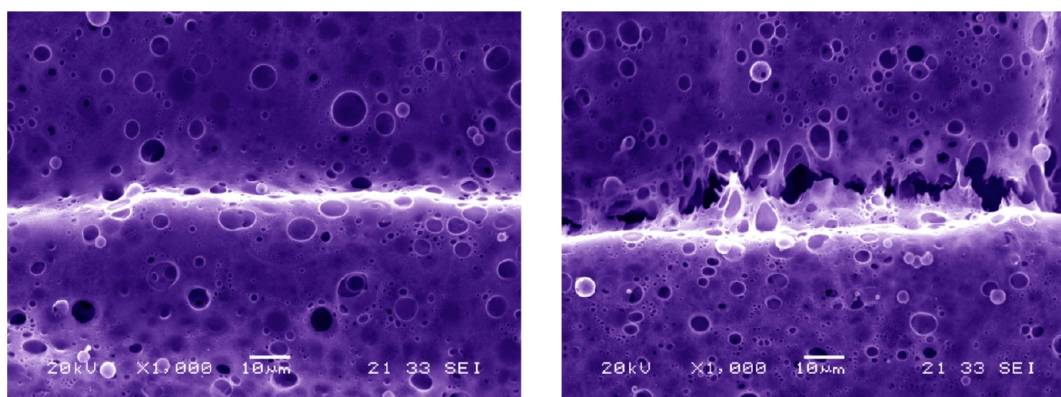
Figure 10. SEM micrographies of PC-1%CNT (20 layers) sensor deposited onto a SoftNorlam sail sample before (left) and after (right) fracture.

fit experimental data as shown in Figure 11 and evaluate both average and ultimate CNT/CNT gaps, respectively $s_0 = 0,503$

Figure 11. Comparison of experimental piezo-reisitive behavior of PC-1%-CNT (40 layers) and fitted with Knite's model until breakage.

nm and s_u = 0.625 nm. These values are in good agreement with that of literature for the inter penetration distance of two carbon atoms, roughly equal to 0.2 nm, and the cut off distance at which tunnelling effect disappears, about 1.8 nm.

4. CONCLUSION

Different strain sensing skins have been developed by spraying LbL directly CPC solutions onto boat sail samples to monitor their deformation. Three kinds of CPC with hierarchical structures (characterized by OM and SEM) were obtained by dispersing CNT into three amorphous thermoplastic matrices (PMMA, aPS & PC). Their performances (sensitivity, reproducibility) have been compared for different values of adjustable parameters such as CNT contents and number of sprayed layers. Although all CPC sensors were able to monitor the strain of the sandwich textile substrate, PC-1%CNT led to the best compromise of properties and was selected for further investigations. Particularly, submitting this CPC sensor to loading/unloading cycles allowed to determine that sensing skins could be used in two different way: under the limit of elasticity of the matrix to follow strain with high reproducibility and over to evaluate the damage accumulation in a non reversible evolution. These results demonstrate the interesting prospects of quantum resistive CPC sensors for strain sensing of sails deformation but also many other kinds of substrates submitted to mechanical solicitations. The great versatility of the technique results from the numerous adjustable parameters such as transducer's thickness, composition and initial resistance, which allow to cover a wide range of piezo-resistive properties, all of this without the use of any thermal treatment, patterning, clean room, etc. Additionally, one major advantage of the process is that transducer's CNT conducting network can be structured in 3D on almost any kind of substrate (even rough textiles) without glue or intermediate substrate. Depending on formulation, the skin sensors can monitor both small strains and plastic deformations until fractures initiate. Compared to metal foil, CPC sensors are cheaper, can be used to map large surfaces by an assembly in network. These sensors are also less sensitive to corrosion and do not need any intermediate glue to transfer the stress. Moreover, the range of deformation accessible to CPC sensors is much larger that their metallic homologues. This can open the door to large scale development of low-cost strain sensors.

■ AUTHOR INFORMATION

Corresponding Author
*E-mail: jean-francois.feller@univ-ubs.fr.

Notes
The authors declare no competing financial interest.

■ ACKNOWLEDGMENTS

■ REFERENCES

(1) Radushkevich, L. V.; Lukyanovich, M. V. *J. Phys. Chem. (Moscow)* **1952**, *26*, 88−95.
(2) Iijima, S. *Nature* **1991**, *354*, 56−58.
(3) Yao, Z.; Kane, C. L.; Dekker, C. *Phys. Rev. Lett.* **2000**, *84*, 2941−2944.
(4) Ding, M. Q.; Shao, W. S.; Li, X. H.; Bai, G. D.; Zhang, F. Q.; Li, Y. H.; Feng, J. J. *Appl. Phys. Lett.* **2005**, *87*, 233118.
(5) Coleman, J. N.; Lotya, M.; O'Neill, A.; Bergin, S. D.; King, P. J.; Khan, U.; Young, K.; Gaucher, A.; De, S.; Smith, R. J.; Shvets, I. V.; Arora, S. K.; Stanton, G.; Kim, H. Y.; Lee, K.; Kim, G. T.; Duesberg, G. S.; Hallam, T.; Boland, J. J.; Wang, J. J.; Donegan, J. F.; Grunlan, J. C.;

3515

dx.doi.org/10.1021/am300594t | *ACS Appl. Mater. Interfaces* 2012, 4, 3508−3516

Moriarty, G.; Shmeliov, A.; Nicholls, R. J.; Perkins, J. M.; Grieveson, E. M.; Theuwissen, K.; McComb, D. W.; Nellist, P. D.; Nicolosi, V. *Science* **2011**, *331*, 568−571.

(6) Treacy, M. M. J.; Ebbesen, T. W.; Gibson, J. M. *Nature* **1996**, *381*, 678−680.

(7) Dai, H.; Rinzler, A. G.; Nikolaev, P.; Thess, A.; Colbert, D. T.; Smalley, R. E. *Chem. Phys. Lett.* **1996**, *260*, 471−475.

(8) Hernadi, K.; Gaspar, A.; Seo, J. W.; Hammida, M.; Demortier, A.; Forro, L.; Nagy, J. B.; Kiricsi, I. *Carbon* **2004**, *42*, 1599−1607.

(9) Gibson, R. F. *Compos. Struct.* **2010**, *92*, 2793−2810.

(10) Adhikari, B.; Majumdar, S. *Prog. Polym. Sci.* **2004**, *29*, 699−766.

(11) Asai, S.; Sumita, M. *J. Macromol. Sci. B Phys.* **1995**, *34*, 283−294.

(12) Ghosh, S.; Sood, A. K.; Kumar, N. *Science* **2003**, *299*, 1042−1044.

(13) Shiba, K. *Science* **2007**, *7*, 285−303.

(14) Tisch, U.; Haick, H. *MRS Bull.* **2010**, *35*, 797−803.

(15) Zee, F.; Judy, J. W. *Sens. Actuators, B* **2001**, *72*, 120−128.

(16) Castro, M.; Kumar, B.; Feller, J. F.; Haddi, Z.; Amari, A.; Bouchikhi, B. *Sens. Actuators, B* **2011**, *159*, 213−219.

(17) Xiaojun, W.; Chung, D. D. L. *Compos. B* **1998**, *29*, 63−73.

(18) Xiaojun, W.; Chung, D. D. L. *Compos. Interfaces* **1998**, *5*, 277−281.

(19) Mei, Z.; Guerrero, V. H.; Kowalik, D. P.; Chung, D. D. L. *Polym. Compos.* **2002**, *23*, 697−701.

(20) Chung, D. D. L.; Wang, S. *Polym. Compos.* **2003**, *11*, 515−525.

(21) Broadbent, S. R.; Hammersley, J. M. *Proc. Camb. Philos. Soc.* **1957**, *53*, 629−641.

(22) Benoit, J. M.; Corraze, B.; Chauvet, O. *Phys. Rev. B* **2001**, 241405.

(23) Droval, G.; Feller, J. F.; Salagnac, P.; Glouannec, P. *Smart Mater. Struct.* **2008**, *17*, 25011.

(24) Zribi, K.; Feller, J. F.; Elleuch, K.; Bourmaud, A.; Elleuch, B. *Polym. Adv. Technol.* **2006**, *17*, 727−731.

(25) Chen, Y. M.; Lai, Y. T.; Yang, Y. J. *Mater. Lett.* **2011**, *65*, 3533−3536.

(26) Feller, J. F.; Grohens, Y. *Sens. Actuators, B* **2004**, *94*, 231−242.

(27) Cochrane, C.; Koncar, V.; Lewandowski, M.; Dufour, C. *Sensors* **2007**, *7*, 473−492.

(28) Cochrane, C.; Lewandowski, M.; Koncar, V. *Sensors* **2010**, *10*, 8291−8303.

(29) Alexopoulos, N. D.; Bartholome, C.; Poulin, P.; Mariolo-Riga, Z. *Compos. Sci. Technol.* **2010**, *70*, 260−271.

(30) Alexopoulos, N. D.; Bartholome, C.; Poulin, P.; Mariolo-Riga, Z. *Compos. Sci. Technol.* **2010**, *70*, 1733−1741.

(31) Kim, K. J.; Yu, W. R.; Lee, J. S.; Gao, L.; Thostenson, E. T.; Chou, T. W.; Byun, J. H. *Compos. A* **2010**, *41*, 1531−1537.

(32) Zhang, R.; Deng, H.; Valenca, R.; Jin, J.; Fu, Q.; Bilotti, E.; Peijs, T. *Sens. Actuators, A* **2012**, *179*, 83−91.

(33) Fan, Q.; Qin, Z.; Gao, S.; Wu, Y.; Pionteck, J.; Mäder, E.; Zhu, M. *Carbon* **2012**, DOI: 10.1016/j.carbon.2012.04.056.

(34) Wicks, S. S.; Guzman de Villoria, R.; Wardle, B. L. *Compos. Sci. Technol.* **2010**, *70*, 20−28.

(35) Thostenson, E. T.; Li, C.; Chou, T. W. *Compos. Sci. Technol.* **2005**, *65*, 491−516.

(36) Li, C. Y.; Thostenson, E. T.; Chou, T. W. *Compos. Sci. Technol.* **2008**, *68*, 1227−1249.

(37) Chou, T. W.; Gao, L.; Thostenson, E. T.; Zhang, Z.; Byun, J. B. *Compos. Sci. Technol.* **2010**, *70*, 1−19.

(38) Li, C.; Chou, T. W. *Compos. Sci. Technol.* **2008**, *68*, 3373−3379.

(39) Thostenson, E. T.; Chou, T. W. *Adv. Mater.* **2006**, *18*, 2837−2841.

(40) Thostenson, E. T.; Chou, T. W. *Nanotechnol.* **2008**, *19*, 215713.

(41) Boger, L.; Wichmann, M. H. G.; Meyer, L. O.; Shulte, K. *Compos. Sci. Technol.* **2008**, *68*, 1886−1894.

(42) Gao, L.; Thostenson, E. T.; Zhang, Z.; Chou, T. W. *Carbon* **2009**, *47*, 1381−1388.

(43) Feller, J. F.; Grohens, Y. *Synth. Met.* **2005**, *154*, 193−196.

(44) Feller, J. F.; Guézénoc, H.; Bellégou, H.; Grohens, Y. *Macromol. Symp.* **2005**, *222*, 273−280.

(45) Decher, G. *Science* **1997**, *277*, 1232−1237.

(46) Mamedov, A. A.; Kotov, N. A.; Prato, M.; Guldi, D. M.; Wicksted, J. P.; Hirsch, A. *Nat. Mater.* **2002**, *1*, 190−194.

(47) Park, Y. T.; Ham, A. Y.; Grunlan, J. C. *J. Phys. Chem. C* **2010**, *114*, 6325−6333.

(48) Tang, Z.; Kotov, N. A.; Magonov, S.; Oztuki, B. *Nat. Mater.* **2003**, *2*, 413−418.

(49) Priolo, M. A.; Gamboa, D.; Grunlan, J. C. *ACS Appl. Mater. Interfaces* **2010**, *2*, 312−320.

(50) Loh, K. J.; Kim, J.; Lynch, J. P.; Kam, N. W. S.; Kotov, N. A. *Smart Mater. Struct.* **2007**, *16*, 429−438.

(51) Pillin, I.; Pimbert, S.; Feller, J. F.; Levesque, G. *Plast. Rub. Compos.* **2002**, *31*, 300−306.

(52) Zribi, K.; Elleuch, K.; Feller, J. F.; Bourmaud, A.; Elleuch, B. *Polym. Eng. Sci.* **2007**, *47*, 1768−1776.

(53) Lynch, J. P.; Loh, K. J.; Hou, T. C.; Kotov, N. A. *Nanotechnol. Constr.* **2009**, *3*, 303−308.

(54) Akter, T.; Kim, W. S. *ACS Appl. Mater. Interfaces* **2012**, *4*, 1855−1859.

(55) Blanks, R. F.; Prausnitz, J. M. *Ind. Eng. Chem. Fundam.* **1964**, *3*, 1−8.

(56) Van Krevelen, D. W.; Nijenhuis, K. In *Properties of Polymers*, 4th ed.; Elsevier: Amsterdam, 1990, 1−875.

(57) Ham, H. T.; Choi, Y. S.; Chung, I. J. *J. Colloid Interface Sci.* **2005**, *286*, 216−223.

(58) Feller, J. F.; Langevin, D.; Marais, S. *Synth. Met.* **2004**, *144*, 81−88.

(59) Feller, J. F.; Guézénoc, H.; Bellégou, H.; Grohens, Y. *Macromol. Symp.* **2005**, *222*, 273−280.

(60) Lu, J.; Feller, J. F.; Kumar, B.; Castro, M.; Kim, Y. S.; Park, Y. T.; Grunlan, J. C. *Sens. Actuators, B* **2011**, *155*, 28−36.

(61) Kumar, B.; Lu, J.; Castro, M.; Feller, J. F. 2010, *81*, 908-915.

(62) Feller, J. F.; Castro, M.; Kumar, B. In *Polymer−Carbon Nanotube Composites: Preparation, Properties and Applications*, 1st ed.; McNally, T.; Pötschke, P.; Woodhead Publishing: Cambridge, U.K., 2011; Chapter 25, pp 760−803.

(63) Li, C.; Thostenson, E. T.; Chou, T. W. *Appl. Phys. Lett.* **2007**, *91*, 223114.

(64) Hu, N.; Karube, Y.; Yan, C.; Masuda, Z.; Fukunaga, H. *Acta Mater.* **2008**, *56*, 2929−2936.

(65) Gau, C.; Kuo, C. Y.; Ko, H. S. *Nanotechnology* **2009**, *20*, 395705.

(66) Dalmas, F.; Dendievel, R.; Chazeau, L.; Cavaillé, J. Y.; Gauthier, C. *Acta Mater.* **2006**, *54*, 2923−2931.

(67) Hu, N.; Karube, Y.; Arai, M.; Watanabe, T.; Yan, C.; Li, Y.; Fukunaga, H. *Carbon* **2010**, *48*, 680−687.

(68) Gao, X.; Zhang, S.; Mai, F.; Deng, Y.; Deng, H.; Fu, Q. *J. Mater. Chem.* **2011**, *21*, 6401−6408.

(69) Li, C.; Chou, T. W. *Compos. Sci. Technol.* **2008**, *68*, 3373−3379.

(70) Zhang, X. W.; Pan, Y.; Zeng, Q.; Yi, X. S. *J. Polym. Sci. B: Phys.* **2000**, *38*, 2739−2749.

(71) Knite, M.; Ozols, K.; Sakale, G.; Teteris, V. *Sens. Actuators, B* **2007**, *126*, 209−213.

(72) Knite, M.; Teteris, V.; Kiploka, A.; Kaupuzs, J. *Sens. Actuators, B* **2004**, *110*, 142−149.

(73) Knite, M.; Tupureina, V.; Fuith, A.; Zavickis, J.; Teteris, V. *Mater. Sci. Eng., C* **2007**, *27*, 1125−1128.